Master's Thesis

Enhanced microstructural homogeneity of extruded Mg-6Zn-0.5Zr alloy by Ca addition

Chang Hee Hong

Department of Materials Science and Engineering

Graduate School of UNIST

2017

Enhanced microstructural homogeneity of extruded Mg-6Zn-0.5Zr alloy by Ca addition

Chang Hee Hong

Department of Materials Science and Engineering

Graduate School of UNIST

Enhanced microstructural homogeneity of extruded Mg-6Zn-0.5Zr alloy by Ca addition

A thesis
submitted to the Graduate School of UNIST
in partial fulfillment of the
requirements for the degree of
Master of Science

Chang Hee Hong

7. 19. 2017

Approved by

_____

Advisor
Sung Soo Park

Enhanced microstructural homogeneity of extruded Mg-6Zn-0.5Zr alloy by Ca addition

Chang Hee Hong

This certifies that the thesis of Chang Hee Hong is approved.

7. 19. 2017

_____

Advisor: Sung Soo Park

_____

Hu Young Jeong

_____

Jung Gu Lee

Abstract

Commercial Mg-6Zn-0.5Zr (ZK60) alloys with different contents of alloyed Ca were subjected to indirect extrusion processing at an initial temperature of 250 °C and subsequently the effect of Ca alloying on the microstructure of the extruded alloys was investigated with particular emphasis on recrystallization and grain growth during the hot extrusion. It was found that alloying with Ca results in the refinement of recrystallized α-Mg grains and also it contributes to enhancing the homogeneity of grain size in the extruded condition. Besides, two different types of second-phase precipitates, $MgZn_2$ and $Ca_2Mg_6Zn_3$, were found to exist in the Ca-containing ZKX600 alloy, although only $MgZn_2$ precipitates appeared in the ZK60 alloy without alloyed Ca. Such microstructural changes in grain size and its homogeneity attained by Ca addition are mainly attributed to the presence of $Ca_2Mg_6Zn_3$ precipitates, which appear to have better thermal stability than $MgZn_2$ precipitates.

Contents

List of figures

Fig. 16. SEM and optical micrographs of the extruded alloys (a,d) before and (b,c,e,f) after heat-treatment at 330 °C for 2 min: (a-c) ZK60 and (d-f) ZKX600.

List of table

Ⅰ. Introduction

Since Mg and its alloys are the lightest structural metals, they are of interest to the automobile industry as a means of reducing the weight of vehicles, thereby the reducing greenhouse gas emissions. [1-3]. In addition, due to the excellent castability of Mg alloys, most automobile parts, such as engine blocks and wheels, are usually fabricated in the form of die castings [4]. For wide application in structural metals, the mechanical properties of Mg alloys must be good enough to satisfy both reliability and safety requirements. However, the low strength of cast Mg alloys limits their applications [5]. Generally, it is well known that wrought processing can enhance the mechanical properties of cast Mg alloys through dynamic recrystallization (DRX), resulting in grain refinement [1].

1.1. Binary Mg-Zn alloy

Binary Mg-Zn alloy is a precipitation hardenable alloy. Fig. 1 shows an equilibrium binary Mg-Zn phase diagram. The maximum solid solubility of Zn in Mg is about 6.2 wt.% at 340 °C and decreases substantially with temperature decreases. In equilibrium state, when Mg_7Zn_3 phase is formed at 340 °C and solidifies at 325 °C or lower, MgZn phase precipitates in Mg + MgZn regions. The precipitation process is complex and takes four steps in Mg-Zn alloy. The precipitation process of Mg-Zn alloy during isothermal aging is shown in Table 1. Binary Mg-Zn alloy may involve the formation of Guinier-Preston (GP) zones, metastable β'_1 (Mg_4Zn_7), β'_2 ($MgZn_2$), and eventually the equilibrium β (MgZn) phase. Maximum hardness is associated with the presence of coherent $MgZn_2$ phase. In the case of the extruded state, hot cracking on the surface can occur at temperatures below the solidus temperature of an alloy during extrusion due to MgZn phase having a low incipient melting point in its as-cast state. To overcome this issue, a homogenization heat treatment is typically applied before extrusion. Metastable $MgZn_2$ phase is formed via dynamic precipitation during extrusion, instead of MgZn.

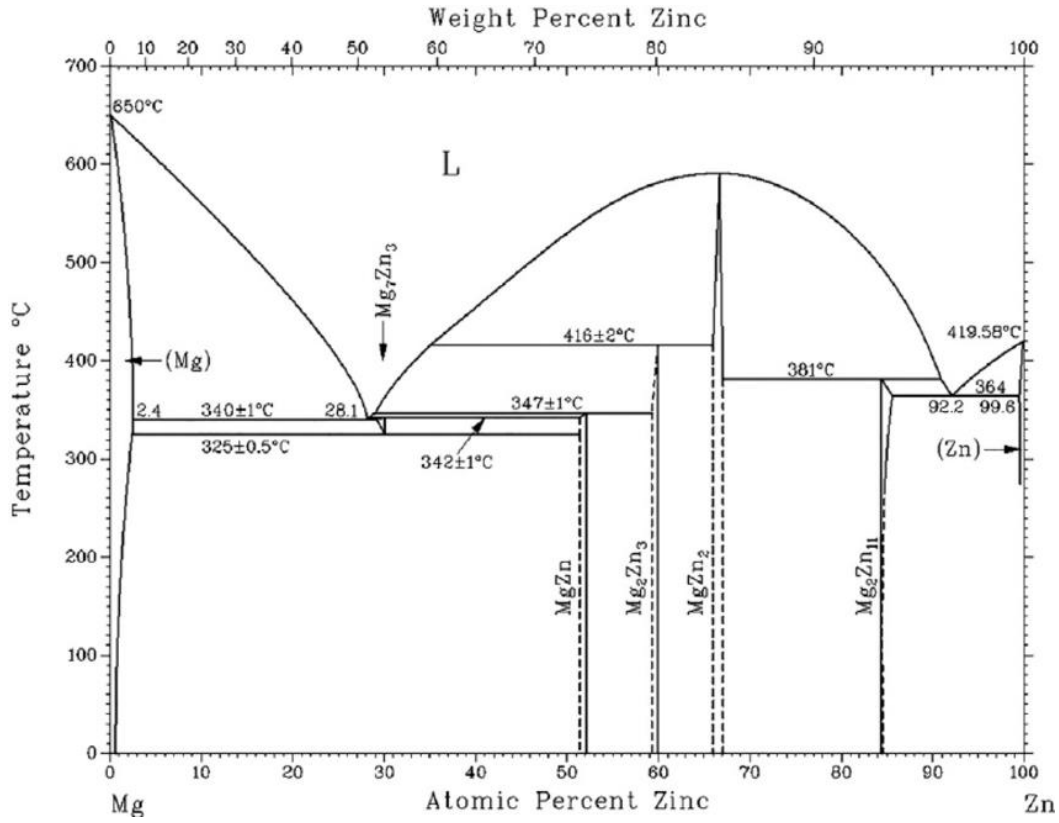

Fig. 1 Equilibrium binary Mg-Zn phase diagram.

Table 1 The precipitation process during isothermal aging of Mg-Zn alloy system [6].

Alloy system	Precipitation process
Mg-Zn	SSSS → G.P. zones → β'_1 (Mg_4Zn_7) → β'_2 ($MgZn_2$) → β (MgZn) $[0001]_\alpha$ rod $(0001)_\alpha$ plate

1.2. Mg-Zn-Zr alloy

Mg-Zn-based ZK60 alloy has been widely used in extruded products due to it having a high tensile yield strength of 255 MPa and a high ultimate tensile strength of 324 MPa [7] compared to the commercial Mg-Al-based alloys [3]. Zr, in particular, has been widely used as a grain refining element for enhancing strength in Mg-Zn-based alloy [8]. For example, it is reported that the extruded Mg-6.2Zn alloy enhances tensile strength by adding Zr [9]. It is attributed to grain refinement and fine β'_1 ($MgZn_2$) precipitates distributed in the matrix as well as along the grain boundaries [9].

However, there is a large microstructural difference in the extruded Mg-Zn alloy with and without Zr. Even though ZK60 alloy has a fine-grained microstructure compared to Zr-free Mg-Zn binary alloy, ZK60 alloy shows a locally inhomogeneous microstructure, whereas extruded Mg-Zn alloy has a uniform microstructure [10].

Although many studies have been conducted on extruded ZK60 alloy, the microstructure inhomogeneity of its alloy has not been studied so far.

1.3. Ca added Mg-Zn-based alloys

Currently, many studies have been conducted on extruded Mg-Zn-based alloys containing a small amount of Ca [10-17]. Y.Z. Du et al. reported that increasing the Ca content up to 0.8 wt.% significantly refined the microstructure of extruded Mg-6Zn alloys. enhancing tensile properties, which increased from 125 MPa to 230 MPa while the ultimate tensile strength increased from 230 MPa to 304 MPa [10]. Also, after extrusion, there is a larger amount of precipitates in the Ca containing Mg-Zn binary alloy.

In addition, ternary $Ca_2Mg_6Zn_3$ phase is formed in the Mg-Zn-Ca based alloy [18, 19], which is mainly located at dynamic recrystallized (DRXed) grain boundaries due to the dynamic precipitation during extrusion [10, 20, 21]. It is reported that fine intermetallic particles precipitated dynamically at the grain boundaries could effectively retard the grain growth during extrusion [22]. Consequently, the $Ca_2Mg_6Zn_3$ phase present at the grain boundary could improve the mechanical properties due to the grain refinement [10].

Furthermore, C.J. Bettles et al. reported that the addition of both Ca and Zr to a cast Mg-4Zn alloy leads to an enhanced age-hardening response and improved mechanical properties at elevated temperature, and superior creep resistance [23].

Although many studies about the extruded Mg-Zn-Ca based alloys and ZK60 alloys with RE element addition have continued to the present [7, 24-33], the effect of Ca addition on the microstructure in the extruded ZK60 alloys has not been studied yet.

Thus, in the present study, commercial Mg-6Zn-0.5Zr (ZK60) alloy and its alloy containing 0.2 wt.% Ca, was subjected to indirect extrusion. The reason for ZK60 alloy's inhomogeneous microstructure and the effect of Ca addition on the microstructure was investigated.

Ⅱ. Background

Wrought processing is the most effective way to enhance strength and ductility of Mg alloys; particularly, severe plastic deformation (SPD), such as equal channel angular processing [34] and high pressure torsion [35]. However, SPD cannot be commercialized as large structural products. For a widespread application of Mg alloys, the extrusion process has been used as industrially available means to improve mechanical properties of Mg alloys via DRX.

2.1. Extrusion

The consumption of magnesium alloys for structural applications has seen considerable growth over the past decade, particularly in the form of die casting. This has been driven primarily by the automotive industry in which the low density of magnesium serves to reduce the weight of vehicles to increase fuel efficiency and to reduce greenhouse gas emission. To expand the application of Mg alloys to more automotive parts, there is a great need for developing wrought magnesium alloys to provide enhanced mechanical properties. The comparison of mechanical properties between cast and wrought alloys is listed in Table 2.

One of the processing methods, extrusion, can enhance mechanical properties of cast Mg alloys through DRX, resulting in grain refinement.

Extrusion is the process whereby a billet is squeezed by a ram in cross-section by pushing it to flow through a die under high pressure. The key advantages of the extrusion process over other processes are its ability to produce extruded bars of complex shapes, and to work metals that are brittle, because the metal is subject to only compressive and shear stresses.

Table 2 Comparison of mechanical properties of automotive materials [3].

Process	Alloy	Density (d, g/cm^3)	Elastic modulus (E, GPa)	Yield strength (YS, MPa)	Ultimate tensile strength (UTS, MPa)	Elongation (e_f, %)	Fatigue strength (S_f, MPa)
Die cast	AZ91	1.81	45	160	240	3	85
Die cast	AM50	1.77	45	125	210	10	85
Extrusion	AZ80-T5	1.80	45	275	380	7	180
Sheet	AZ31-H24	1.77	45	220	290	15	120

(T5 signifies artificially aged after extrusion. H24 signifies strain hardened and partially annealed.)

2.2. Types of extrusion process

2.2.1. Direct extrusion

The direct extrusion process is illustrated in Fig. 2 (a). It is well known as the most common extrusion process. When the billet is placed into a container and a ram compresses the billet, it begins to flow through the die at the opposite end of the container. As the ram reaches the die, the end of the billet that cannot be pushed through the die remains. However, the major problem of direct extrusion is that there is significant friction generated between the metal surface and the walls of the container as the billet is pushed toward the die. This is directly related to low extrusion speed, because it is likely to cause surface cracking during extrusion, resulting from the second-phase particles which have a low incipient melting point. In addition, the ram force required for direct extrusion significantly increases friction and generates the grain growth of DRXed microstructure.

2.2.2. Indirect extrusion

The indirect extrusion process is illustrated in Fig. 2 (b). the hollow ram is moved by forcing it to flow though the die while the billet is kept stationary. Since the billet is not forced to move, there is less friction at the container walls compared to direct extrusion, and the ram force required to extrude the billet is lower than in direct extrusion. Therefore, the indirect extrusion process facilitates more rapid extrusion and more refinement of the DRXed microstructure than direct extrusion process.

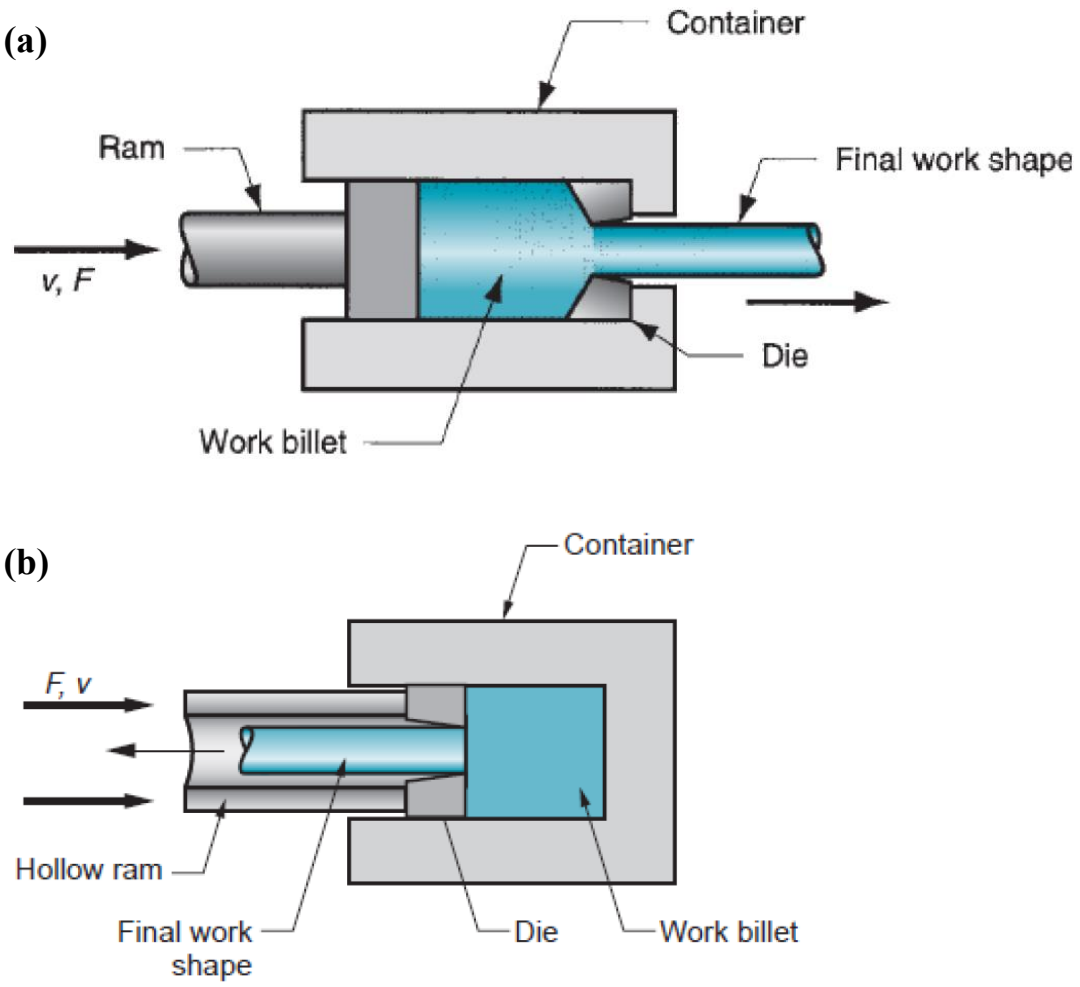

Fig. 2. Types of extrusion process: (a) direct extrusion and (b) indirect extrusion.

2.3. Dynamic recrystallization

In general, recovery and recrystallization can take place during post-deformation heat treatment. However, in the event of recovery and recrystallization associated with deformation, it is called dynamic recovery and dynamic recrystallization (DRX). Recovery can occur in metals such as pure Al and Al alloys which have high stacking fault energy due to the dislocation climb and cross slip. In metals of lower stacking fault energy such as copper, nickel and austenite iron, recovery is slow and the dislocation density increases the critical value necessary for DRX.

DRX may operate during hot working, such as extrusion, rolling and forging, and static recrystallization may occur by residual heat, as shown in Fig. 3. DRX generally originates at high angle boundaries. As the metals continue to deform, newly dynamic recrystallized (DRXed) grains are nucleated at the old grain boundaries, the dislocation density of the newly DRXed grains increases, thus reducing the driving force for further growth, and the DRXed grains eventually stop growing.

Fig. 4. shows the development of microstructure during DRX. DRX generally originates at the old grain boundaries, as seen in Fig. 4 (a) and (b). In this way, DRX continues to occur around the newly DRXed grain, thickening the band of DRXed grains, as shown in Fig. 4 (c). The metal eventually becomes fully recrystallized, as in Fig. 4 (d).

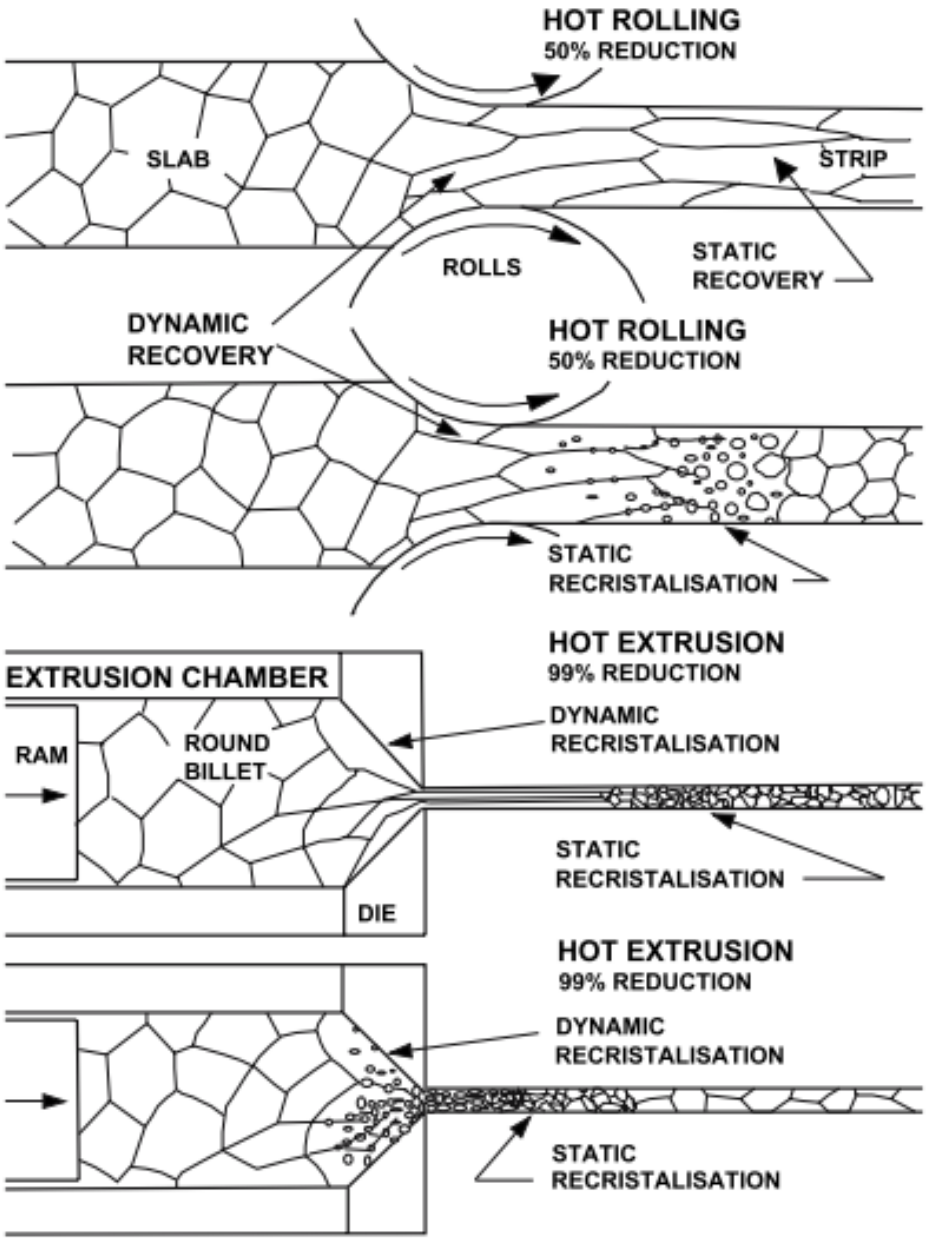

Fig. 3 Schematic illustration of possible softening process during hot-working [36].

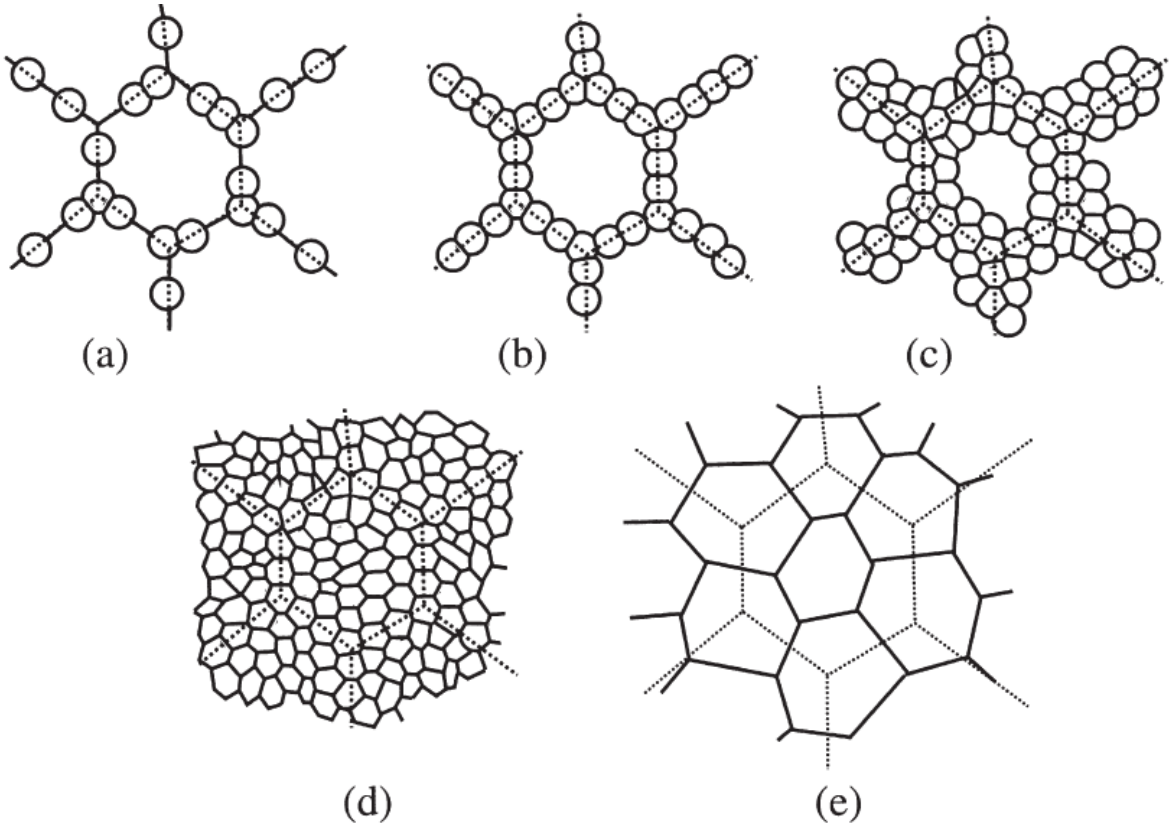

Fig. 4 Microstructural development during DRX: (a-d) Large initial grain size, (e) small initial grain size. The dotted lines show the prior grain boundaries. [37]

2.4. Microstructural evolution during extrusion; the case of Mg-3Al-1Zn alloy

In the extruded microstructure, particularly, grain size is directly related to the mechanical properties of wrought Mg alloy.

During the extrusion process of Mg alloys, DRX operates during hot extrusion and a fine-grained microstructure is developed. This process can be seen in Fig. 5, which shows the microstructural development in extruded Mg-3Al-1Zn alloy (a finite element method simulation indicating the material flow and strains, is included).

In the low strain region of the billet (Fig. 5 (a)), newly DRXed grains are nucleated at the old grain boundaries, forming a 'necklace' type structure. Twins are also present and in some regions act as nucleation sites for further DRX. In the middle of the billet (Fig. 5 (b)), where the deformation strain is slightly higher, DRXed grains surrounding the old grains and the twins continue to thicken. In the main deformation zone (Fig. 5 (c)), where the strain is the highest, the DRXed fraction increases significantly, thus reducing the overall grain size of the alloy.

Fig. 5 (c) also reveals that, for the imposed extrusion conditions, the microstructure is not completely dynamically recrystallized; the remainders of old grains that did not undergo DRX can be seen as elongated in the extrusion direction (this is a relatively high imposed deformation strain of over four). This behavior is most likely a result of localized deformation. there are no longer nucleation sites once the old grain boundaries have been completely surrounded by the DRXed grains. Such a bimodally grained microstructure consisting of equiaxed DRXed and elongated unDRXed grains has been reported to form when it is not uniformly distributed precipitates in homogenized billet [38].

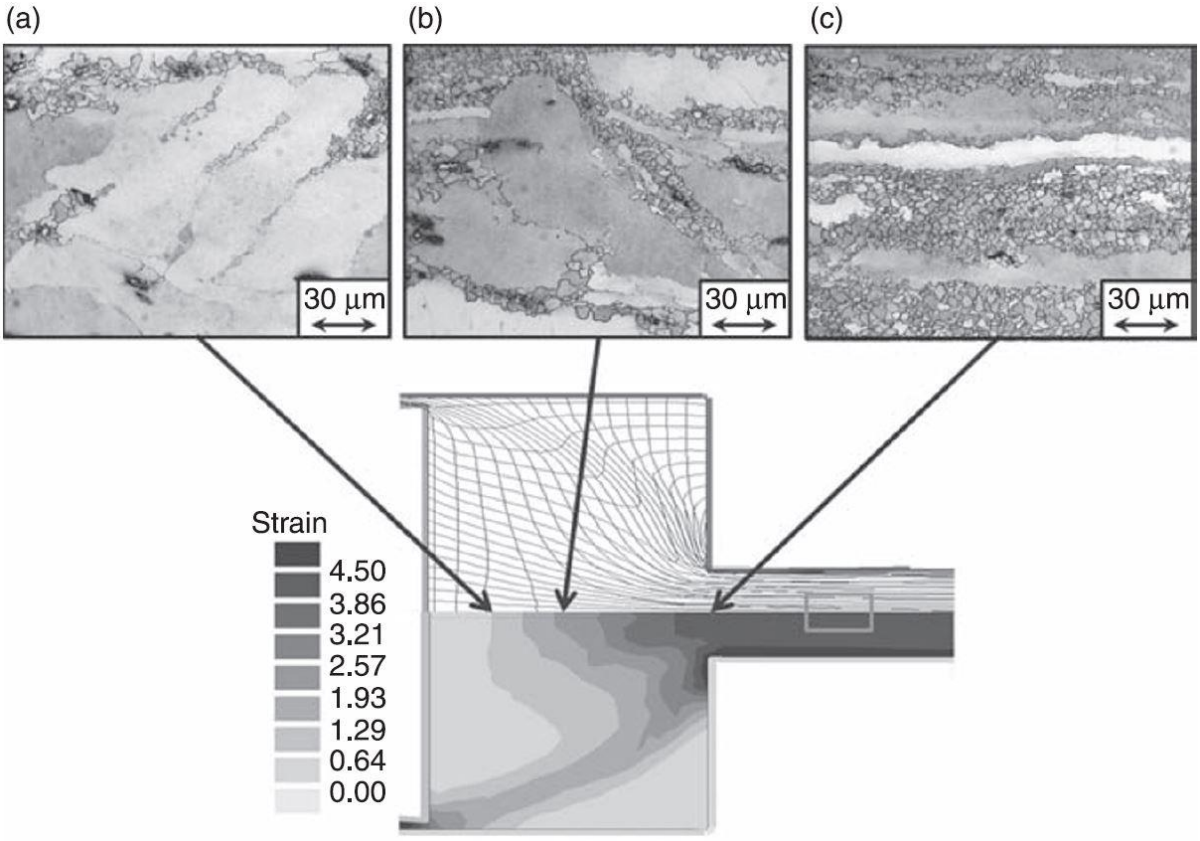

Fig. 5. Microstructure evolved in a partially extruded Mg-3Al-1Zn billet and corresponding a finite element method simulation indicating the flow pattern and strains attained. (T_{ex}=300 °C, V_{ex}=0.01 mm/s, ER=30) [39].

2.5. Dynamic precipitation

Precipitation hardening is an effective way to enhance the mechanical properties of Mg alloys. Many studies have been conducted to enhance the age-hardening response of Mg alloys. i.e. Mg-Al, Mg-Zn-based alloys without deformation. In the case of precipitation associated with deformation, such as extrusion, it is called dynamic precipitation. If the metal is deformed, the stress increases and the dislocations accumulates, so that the precipitation can occur even below the static precipitation temperature. The increase in stress serves to shorten the time required for the nucleation of the precipitate below the recrystallization temperature, and movement of the dislocation during deformation improves the diffusion rate of atoms. In addition, in the case of the deformed region, dynamic precipitates in the DRXed region have a spherical-shape, whereas rod-shaped precipitates in the aged Mg-Zn-based alloys are without deformation [40, 41]. The reason for the formation of spherical precipitates is attributed to the relative soft Mg matrix where fine spherical precipitates may reduce interfacial energy and may not increase strain energy because the characteristics of the interface between precipitates and Mg matrix is incoherent. Meanwhile, the precipitates were precipitated unevenly in wrought Mg alloys through deformation. Although the billet is homogenized prior to hot-working, dynamic precipitation occurs for a short time due to frictional heat generated during hot-working and the precipitates are distributed unevenly. Accordingly, the size distribution of the DRXed grains may be uneven, depending on the non-uniform distribution of the dynamic precipitates.

2.6. Grain boundary pinning

Grain boundary pinning by second-phase particles at the grain boundaries has been widely used to prevent grain growth during heat treatment in Mg alloys.

In wrought Mg alloys, grain growth may occur due to the frictional heat generated during hot extrusion when the billet is deformed. However, fine precipitates can act to prevent the motion of the grain boundaries by exerting a pinning pressure, called Zener pinning. They can eventually inhibit grain growth, leading to the grain refinement [42]. There is SEM micrograph of extruded Mg-5Sn-1Zn-3Al alloy as shown Fig. 6. This is a typical example of causing grain refinement by precipitates present at grain boundaries.

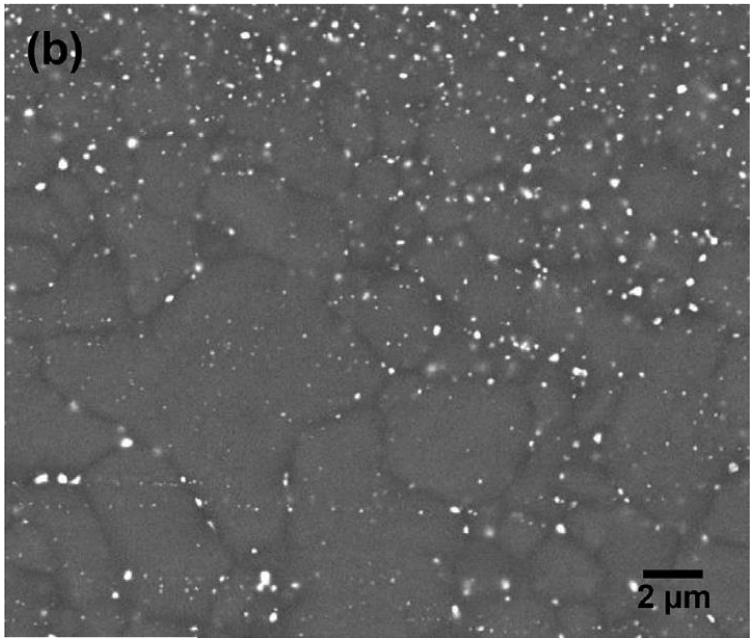

Fig. 6. SEM micrograph of extruded Mg-5Sn-1Zn-3Al alloy [42].

2.6.1. Effect of particles on grain growth

Generally, when recovery and recrystallization are complete, grain growth is caused by migrating grain boundaries at high temperature.

Fig. 7 (a) shows the grain growth behavior when second-phase particles are present in the Mg matrix. As shown in Fig. 7 (a), the moving boundaries become trapped in the particles as the grain grows, so that the particles exert a force to limit the movement of the grain boundary. The boundary shown in Fig. 7 (b) is trapped to the particle with a length of $2\pi r\cos\theta$. Therefore, if the boundary meets the particle surface at an angle θ, the restraining force on the boundary is $(2\pi r\cos\theta\,\gamma)\sin\theta$. The maximum force exerted by a single particle is given by $\pi r\gamma$ when $\sin\theta\cos\theta$ is a maximum, i.e., at θ=45°.

The pressure P will counteract the driving force for grain growth, namely ~$2\gamma/\overline{D}$ as shown in Fig. 7 (a). This pressure means the value multiplied by the maximum force per particle and the number of particles per unit area of the boundary.

As this pressure is identical to the driving force for grain growth, grain boundary migration may be stopped. On the other hand, when P_{max} is smaller than the driving force $2\gamma/\overline{D}$, grain growth may occur.

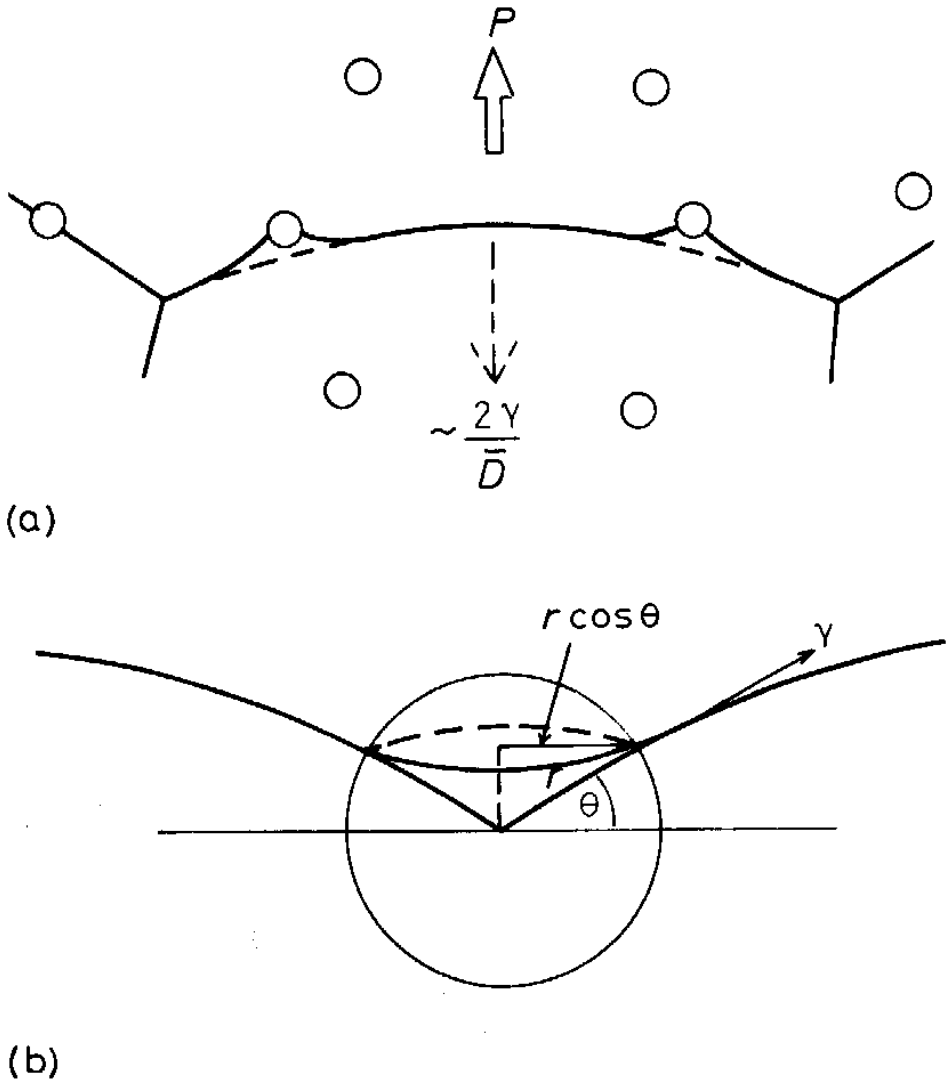

Fig. 7. Effect of spherical particles on grain boundary migration [43].

Ⅲ. Experimental

3.1. Sample preparation

The billets for extrusion with nominal compositions (wt.%) of Mg-6Zn-0.5Zr (ZK60), Mg-6Zn-0.5Zr-0.2Ca (ZKX600) were prepared in a graphite crucible by induction melting. The molten metals were stabilized for 10 min at 700 °C and then poured into a steel mold preheated to 200 °C under an inert atmosphere with a SF_6 and CO_2 mixture. The billets were homogenized at 440 °C for 4 h prior to indirect extrusion and subsequent quenched in water to obtain a supersaturated solid solution. The dimensions of billet were 78 mm in diameter and 100 mm in length. Indirect extrusion were conducted at 250 °C with a ram speed of 0.65 mm s^{-1} and an extrusion ratio of 25 by using indirect extrusion equipment in natural cooling condition, as shown in Fig. 8. The ZK60 and ZKX600 alloys were extruded cleanly without surface cracks, as shown in Fig. 9. In case of ZK60 alloy, these alloy is extruded to approximately 1900 mm, and then, the remaining part of the billet (a size of 20 mm), called the butt, is separated from the extrudate by cutting it just beyond the exit of the die.

3.2. Microstructural examination

Microstructural examination of extruded samples was conducted on the midsections parallel to the extrusion direction (ED). Extruded samples were ground on SiC papers of up to 1200 grits under water-based atmosphere; and then samples were finely polished using 1 μm diamond suspension and 0.04 μm colloidal silica under an alcohol-based atmosphere. These polished samples were chemically etched to observe grain boundaries in a solution consisting of 4.2 g picric acid, 10 ml distilled water, 10 ml acetic acid and 70 ml ethanol. The microstructure of the samples was observed by using optical microscopy (OM; Nikon EPIPHOT 200), scanning electron microscopy (SEM; Quanta 200 field-emission scanning electron microscope), transmission electron microscopy (TEM; FEI-Tecnai G^2 F20) equipped with an energy dispersive spectrometer (EDS) operating at 200 kV. Average grain size of the extruded samples was measured using a linear intercept method; D = 1.74 x L, where D is the grain size and L in the linear intercept size. TEM samples were prepared by jet-polishing method using a solution of 600 ml methanol, 300 ml nitric acid and 100 ml glycerol at about -10 °C and 13 ~ 15 V, and then precisely polished to remove the oxide layer on the surface by ion milling using a Gatan Precision Ion Polishing System (PIPS).

Fig. 8. Appearance of an indirect extrusion equipment.

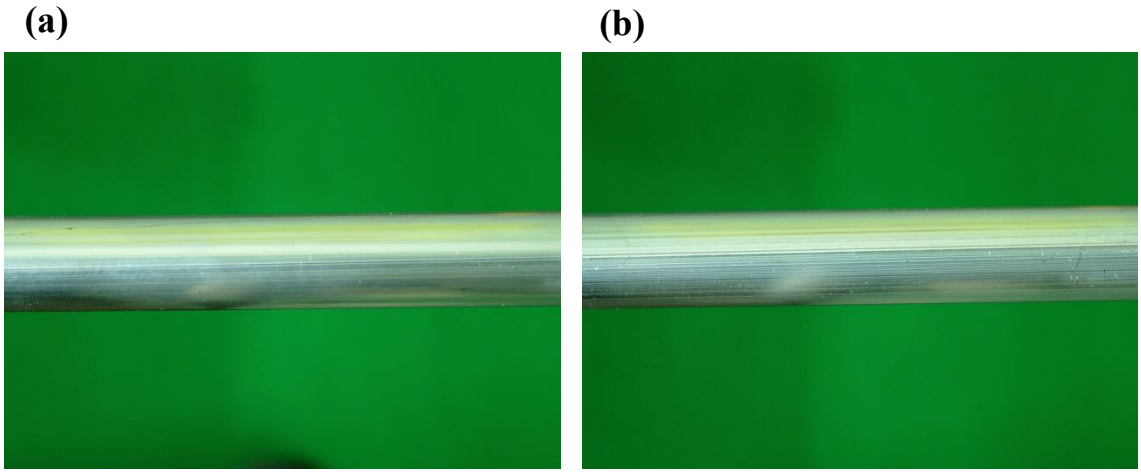

Fig. 9. Surface appearance of extruded bars of the ZK60 and ZKX600 alloy: (a) ZK60 and (b) ZKX600.

Ⅳ. Result

4.1. Microstructure after extrusion

Fig. 10 shows the optical micrographs of the extruded ZK60 and ZKX600 alloys (a plane parallel to the ED). The overall microstructures commonly contained the equiaxed α-Mg grains formed by DRX during extrusion and the elongated unDRXed grains that remain incompletely along ED. Compared to the ZK60 alloy, the microstructure was uniformly distributed by the addition of Ca.

The microstructure of the ZK60 alloy has diverse distribution in DRXed grain size, compared to the ZKX600 alloy i.e. equiaxed DRX grains of the ZK60 alloy exist fine α-Mg grains of ~2 μm and relatively coarse α-Mg grains of 30~80 μm. On the other hand, the DRX microstructure becomes more homogenous with the addition of Ca.

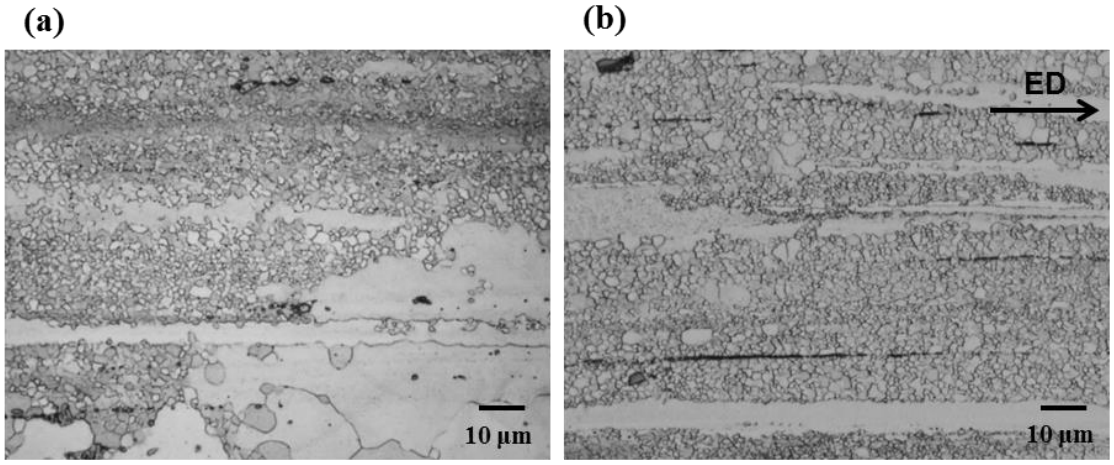

Fig. 10. Optical micrographs of extruded (a) ZK60 and (b) ZKX600 alloys.

The average grain sizes, considering both equiaxed and elongated grains, are 2.6 and 2.1 μm for the ZK60 and ZKX600 alloys, which are slightly decreased from 2.6 to 2.1 μm due to microstructure homogeneity of DRXed regions by Ca addition. The area fractions of the elongated unDRXed grains are 9.4%, 17.8% for the ZK60, ZKX600 alloys, respectively.

In order to observe the amount of dynamic precipitates formed during extrusion in DRXed regions, extruded samples were chemically etched and observed using SEM. Fig. 11 shows SEM micrographs in DRXed regions of the extruded alloys. Dynamic precipitates were commonly distributed to DRXed regions within grain interiors, as well as at grain boundaries. Notably, there was a larger amount of precipitates in the ZKX600 alloy than in those of ZK60.

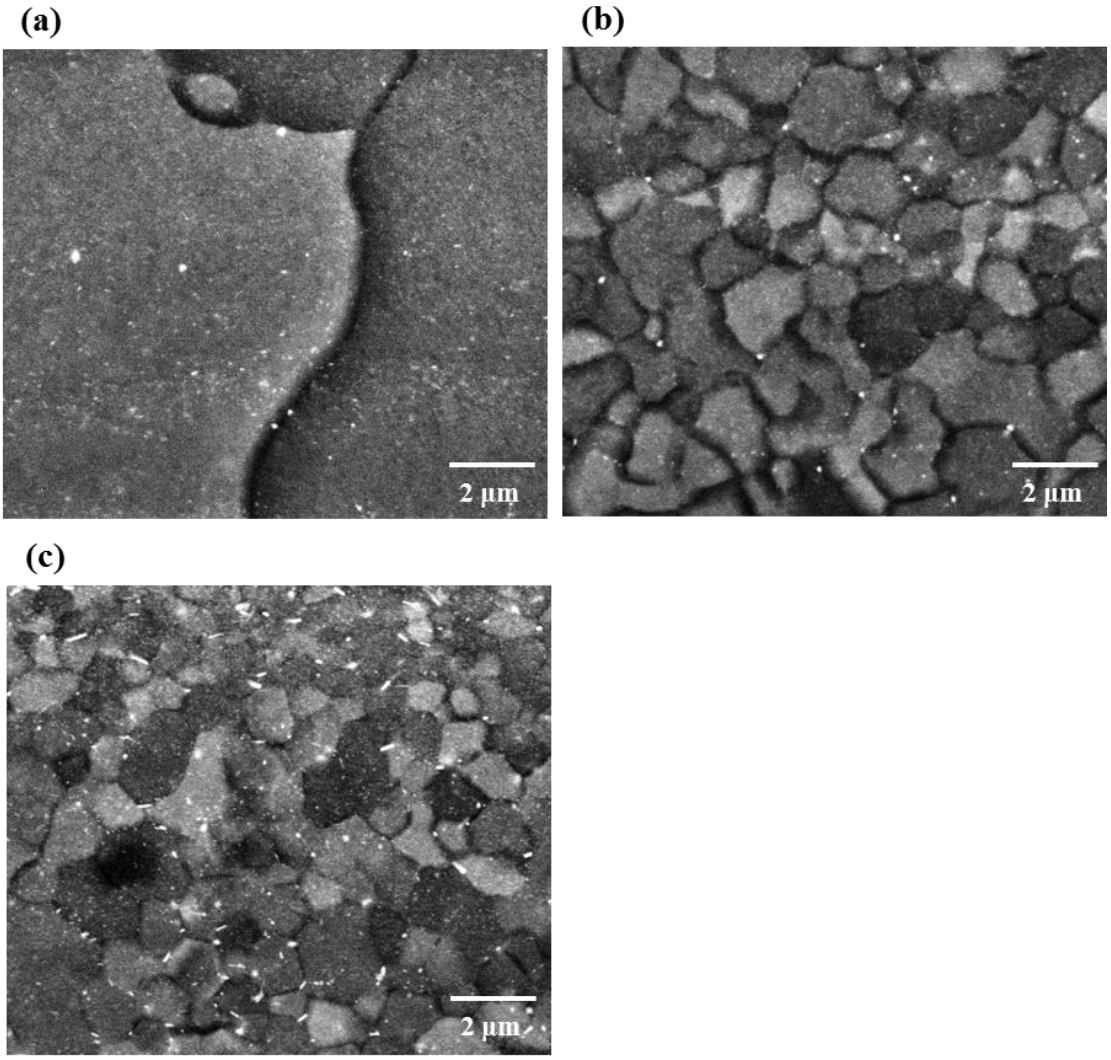

Fig. 11 SEM micrographs in the DRXed regions of extruded ZK60 and ZKX600 alloys: (a-b) ZK60 and (c) ZKX600.

To identify what kinds of precipitates present in SEM micrographs (Fig. 11), TEM analysis of the extruded alloys was performed, as shown in Fig. 12 and 13. Fine spherical precipitates were observed in the extruded alloys. In the TEM bright field image of the ZK60 alloy (Fig. 12), energy dispersive spectrometry (EDS) revealed that the precipitates were present in the form of Mg-Zn with or without Zr. The analysis result of electron diffraction patterns obtained from the Mg-Zn phase, shown in Fig. 12 (c,e), indicates that this phase coincides well with $MgZn_2$, which has a hexagonal closed-packed structure with lattice parameters of a=0.522 nm, c=0.857 nm. In the TEM bright field image of the ZKX600 alloy (Fig. 13), EDS analysis indicates that Zn-Mg-Zr containing 2.1 at.% Ca and Mg-Zn-Ca precipitate containing 3.1 at.% Ca were observed at the DRXed grain boundary. Through the analysis of electron diffraction patterns, the Zn-Mg-Zr and Mg-Zn-Ca phase coincide well with $MgZn_2$ and $Ca_2Mg_6Zn_3$, respectively. $Ca_2Mg_6Zn_3$ phase, which has a hexagonal closed-packed structure with lattice parameters of a=0.973 nm, c=1.015 nm, is newly formed by Ca addition. Fine $MgZn_2$ precipitates were observed in the extruded alloys regardless of Ca addition. $MgZn_2$ precipitates, known to be typically observed in wrought ZK60 alloy [9, 40], are present in the ZKX600 alloy as well. The second-phase particles in the Mg-Zn-Ca alloy have been known to exist in the form of Mg_2Ca or $Ca_2Mg_6Zn_3$, which relies on the atomic ratio of Zn/Ca. $Ca_2Mg_6Zn_3$ phase predominates when the Zn/Ca atomic ratio is greater than 1.23 [44]. Mg_2Ca was not found to exist because the atomic ratio of Zn/Ca of ZKX600 alloy is much higher than the 1.23 [44]. In addition, $Ca_2Mg_6Zn_3$ phase itself has the Zn/Ca atomic ratio of 1.5. However, $Ca_2Mg_6Zn_3$ phase, which is present in ZKX600 alloy, do not have the Zn/Ca atomic ratio of 1.5. Several studies suggest that the Zn/Ca atomic ratio may not be 1.5, depending on the situation [45, 46].

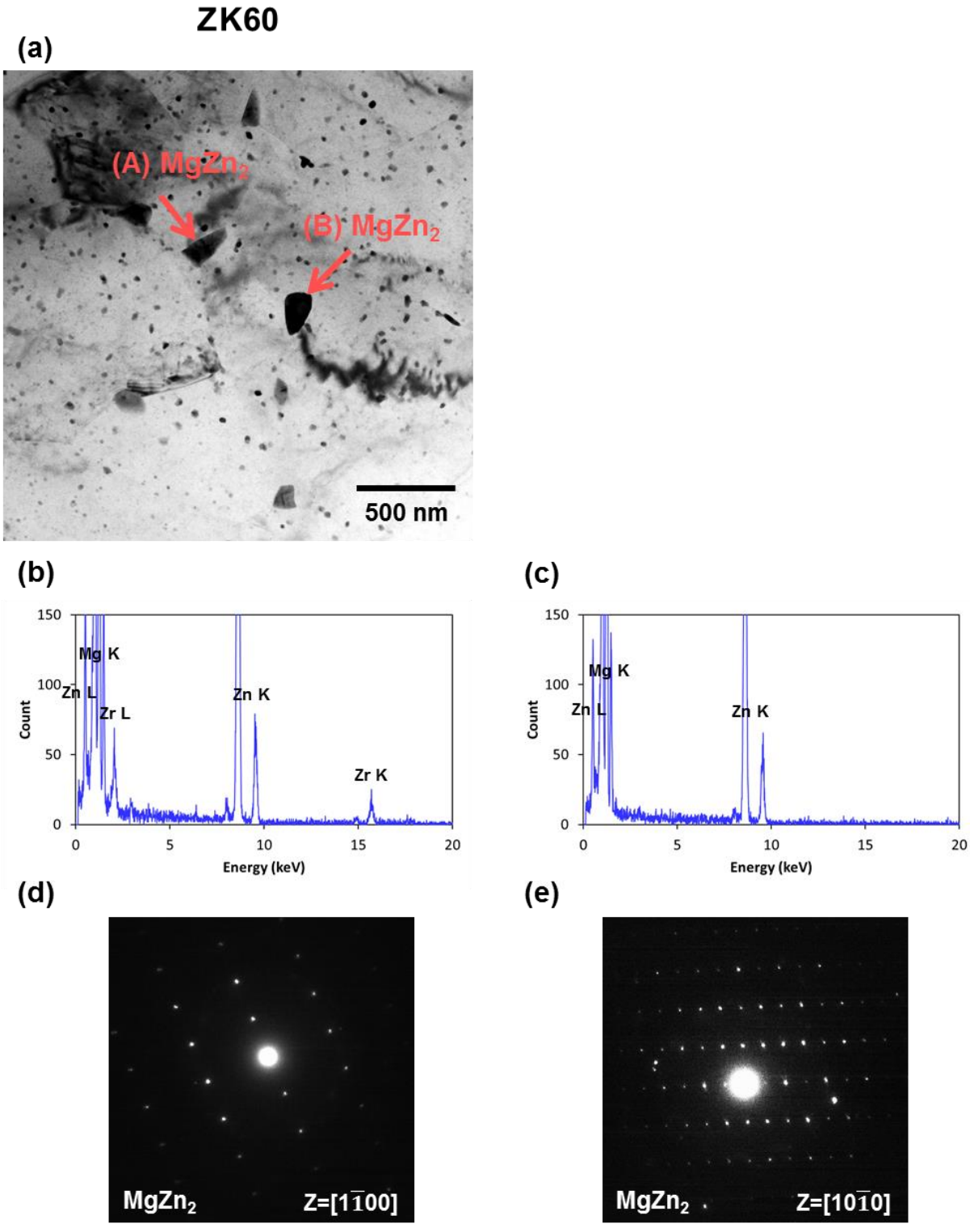

Fig. 12. (a) TEM micrograph, (b,c) EDS spectra, and (d,e) electron diffraction patterns from the (b,d) C and (c,e) D precipitates in the ZK60 alloy.

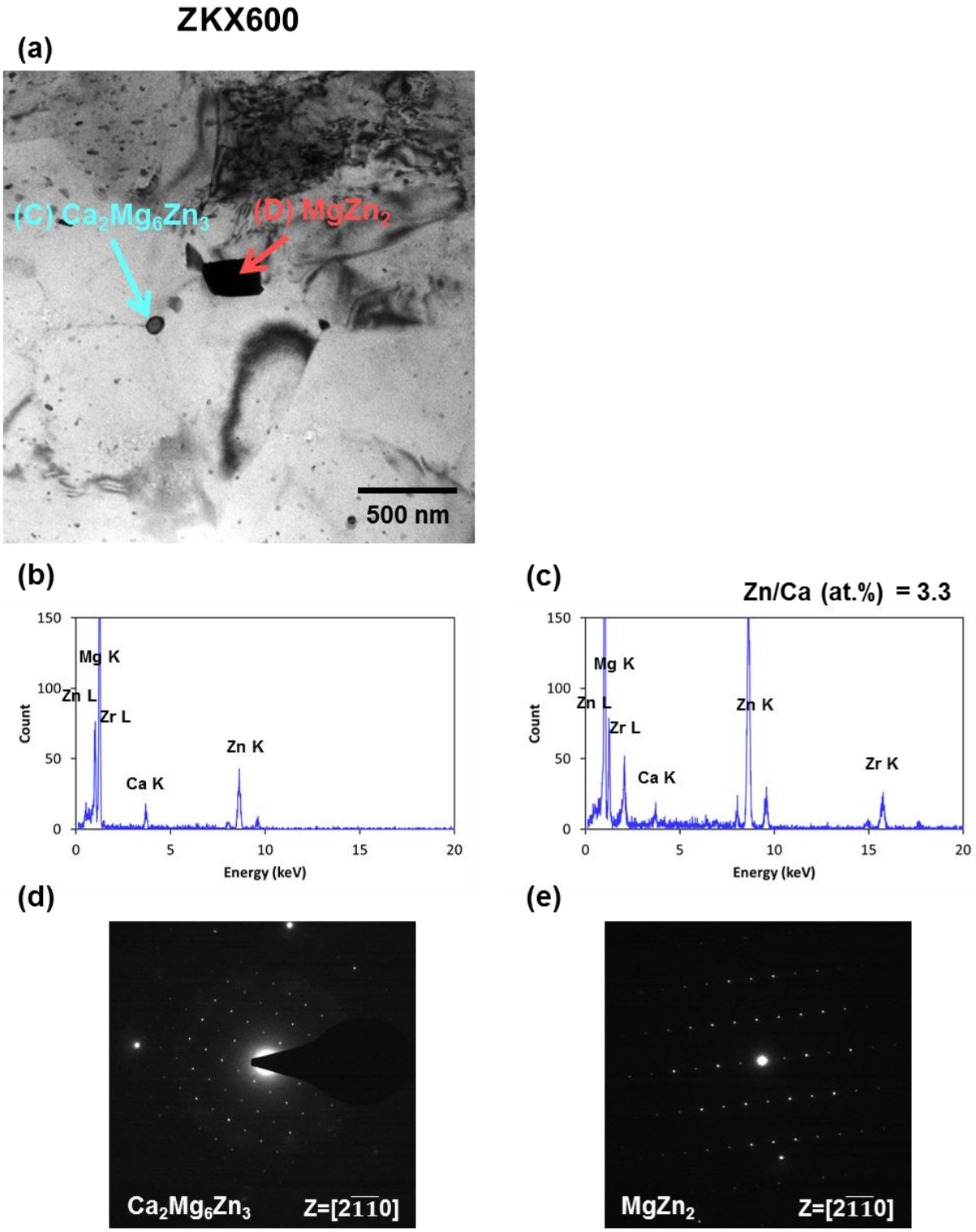

Fig. 13. (a) TEM micrograph, (b,c) EDS spectra, and (d,e) electron diffraction patterns from the (b,d) C and (c,e) D precipitates in the ZKX600 alloy.

4.2. Microstructural evolution during extrusion; case of ZK60 alloy

In order to examine the microstructural evolution during extrusion, the microstructure of the remaining sample after extrusion, known as butt, was observed. The microstructure of each region at the marked points 1-6 in Fig. 14 (a) is also shown in Fig. 14 (b-g). Among them, Fig. 14 (b-d) show optical micrographs before passage through the die. In the initial region of the extrusion (between Fig. 14 (b) and (c)) fine DRXed grains with a size of several microns have been nucleated around old grain boundaries, forming a 'necklace' type structure. Twins are also present and in some regions they have acted as nucleation sites for further DRX. Just before passage through the die (Fig. 14 (d)), the degree of DRX increased significantly and fine DRXed grains surrounding the original grains and twins continued to thicken.

Fig. 14 (e-g) show optical micrographs after passage through the die. The microstructure immediately after extrusion in Fig. 14 (e) consists of fine DRXed grains and elongated unDRXed grains in the ZK60 alloy. However, as billet passed through the die, some of the fine DRXed grains grew up coarsely during extrusion.

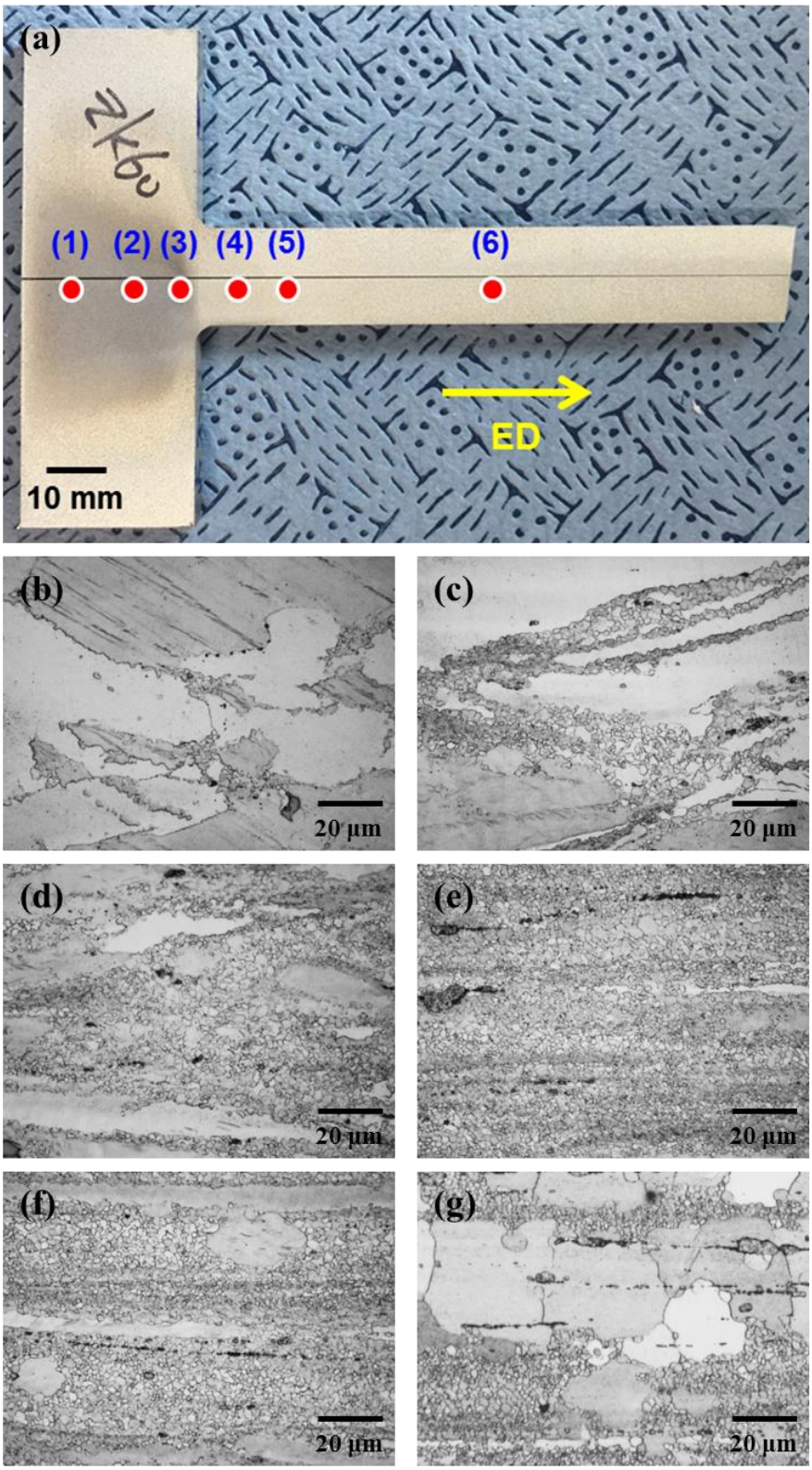

Fig. 14. (a) Macroscopic optical micrograph showing the cross-section of the ZK60 alloy butt and (b-g) optical micrographs taken at the marked points 1-6 in (a).

Ⅴ. Discussion

Overall microstructure of the extruded alloys shows that the microstructural inhomogeneity of ZK60 alloy was enhanced by Ca addition, as shown in Fig. 10. The objective of this study is to investigate the reason why the microstructural inhomogeneity was enhanced by Ca addition and the effect of Ca addition on the microstructure, considering the microstructural factor.

The amount of precipitates increased in the ZKX600 alloy due to Ca addition, as shown in Fig. 11. It may contribute to more homogeneous microstructure because the precipitates at grain boundaries cause grain boundary pinning, inhibiting grain growth. On the other hand, some DRXed grains may grow coarsely in the region where the precipitates of sufficient size to cause grain boundary pinning are relatively less distributed in the ZK60 alloy.

Since ZK60 alloy has two types of DRXed grains, this study attempted to discover why coarse DRXed grains exist in this alloy. In the microstructural evolution until just before extrusion (Fig. 14 (b-f)), the microstructure of ZK60 butt sample showed typical DRX behavior, in which newly DRXed grains are nucleated at old grain boundaries and deformation twins. The microstructure immediately after extrusion in the ZK60 alloy consists of fine DRXed grains and elongated unDRXed grains (Fig. 14 (e)). However, as billet passed through the die, some of fine DRXed grains grew up coarsely to a size of 40 μm. It has often been reported that there appears a bimodal grain size distribution of DRXed grain when it is extruded at a temperature range of 225~300 °C and cooled in air. This is especially observed in the extruded Mg-3Al-1Zn and Mg-6Zn-0.5Zr alloy in natural cooling conditions [47, 48]. On the other hand, it can have homogeneous DRXed grains in the same alloy under different cooling conditions, i.e., the extrusion process is conducted in the same ZK60 alloy with artificial cooling, which can realize low temperature extrusion [48]. It is reported that the temperature measured at the die exit during extrusion is 180 and 290 °C in the samples with and without artificial cooling in the same ZK60 alloy [48]. It is well known to have large DRXed grains due to frictional heat, that has an increasing exit temperature [30]. Accordingly, the reason why DRXed grains grew coarsely in some regions of ZK60 alloy is directly related to high frictional heat generated during extrusion. However, the DRXed grains of the ZKX600 alloy did not grow coarsely despite frictional heat generated during extrusion, as shown in Fig. 10. Moreover, two different types of second-phase precipitates, $MgZn_2$ and $Ca_2Mg_6Zn_3$, were found to exist in the ZKX600 alloy, although only $MgZn_2$ precipitates appeared in the ZK60 alloy, as shown in Fig. 12 and 13. Here, it is important to have thermally stable precipitates in the extruded alloys. If thermal stability of precipitates is low, precipitates inhibiting grain growth are dissolved into the matrix by frictional heat, leading to grain growth. For that reason, non-equilibrium thermodynamic

calculation was conducted to compare thermal stability by using Pandat software between two different types of second-phase precipitates during solidification in the ZKX600 alloy, as shown in Fig. 15.

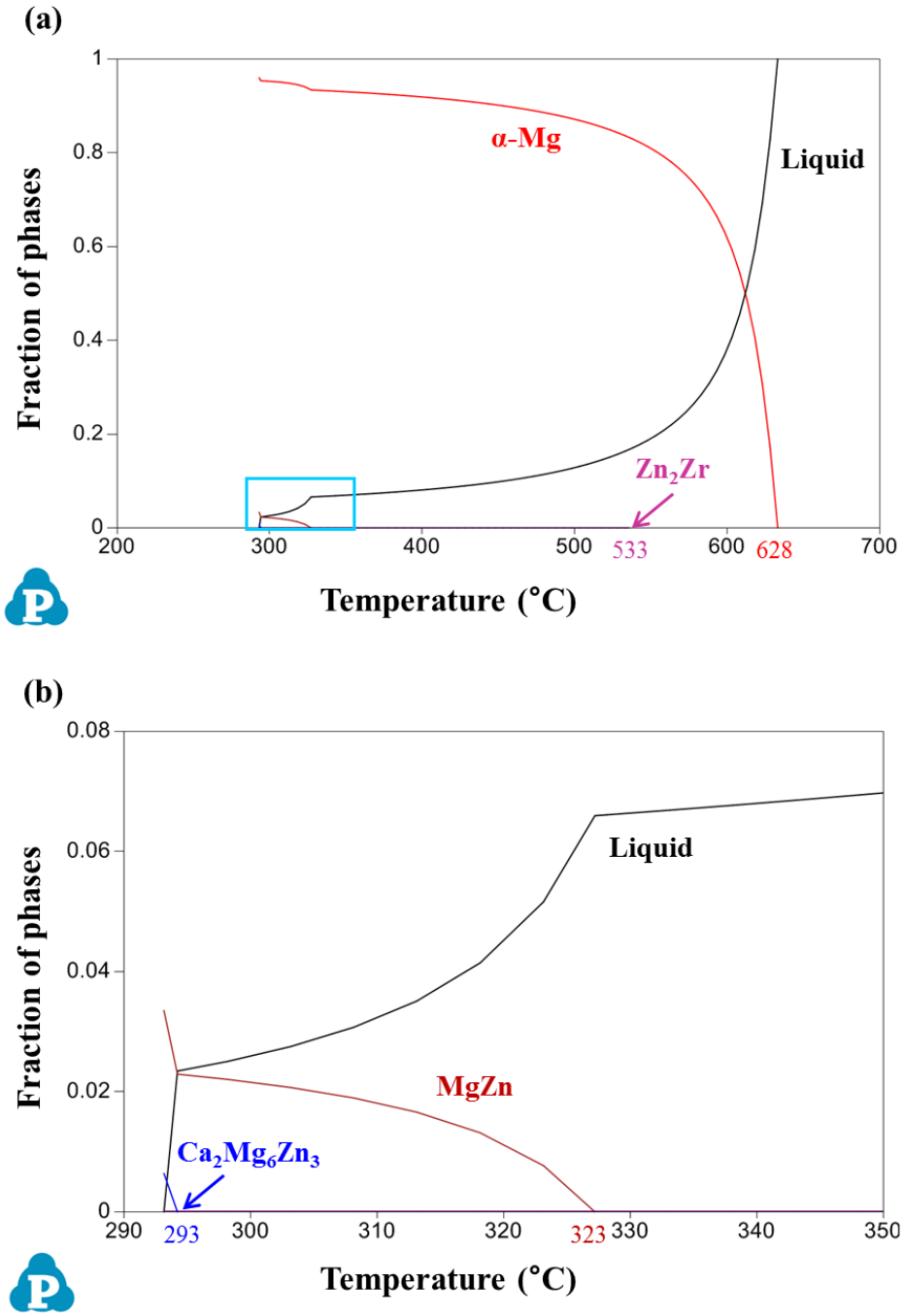

Fig. 15. (a) Non-equilibrium thermodynamic calculation showing the fraction of phases as a function of temperature for the ZKX600 alloy. (b) an enlarged view of the rectangular part shown in (a).

In a non-equilibrium state, when Zn_2Zr phase is formed at 533 °C and solidified below 330 °C, MgZn and $Ca_2Mg_6Zn_3$ phases are formed at 323 and 293 °C, indicating that MgZn phase is thermally more stable than $Ca_2Mg_6Zn_3$ phase, as in Fig. 15. However, during homogenization of a billet prior to extrusion, MgZn phase generated at low temperature is dissolved into the Mg matrix. These phases are is dynamically precipitated in the form of $MgZn_2$ during extrusion, which can be precipitated even below the static precipitation temperature through deformation.

Therefore, in order to determine the thermal stability of dynamic precipitates in the extruded alloys, artificial heat-treatment was conducted for 2 min within the rising temperature range during extrusion. Fig. 16 shows SEM and optical micrographs of the extruded alloys with and without heat-treatment at 330 °C for 2 min. Fine precipitates were commonly found to exist in an as-extruded state of the extruded alloys in Fig. 16 (a) and (d). However, when the temperature was increased to 330 °C in the ZK60 alloy, most of fine precipitates were almost dissolved into the matrix. In addition, the coarse DRXed grains were larger and most of fine DRXed grains grew coarsely, as shown in an optical micrograph of ZK60 alloy (Fig. 16 (c)). This is similar to abnormal grain growth phenomenon. It is well known that abnormal grain growth occurs as the grain growth inhibiting second-phase particles dissolve. TEM analysis of the precipitates (see Fig. 12), identified them as being in the $MgZn_2$ phase. As a result, some of DRXed grains seem to grow coarsely in the ZK60 alloy because the $MgZn_2$ precipitates inhibiting grain growth were almost dissolved into the matrix by frictional heat generated during extrusion.

On the other hand, as mentioned earlier, microstructure of extruded ZKX600 alloy consists of fine DRXed grains with a size of ~2 μm and elongated unDRXed grains, as shown in Fig. 10. This is very similar to the microstructure immediately after extrusion in ZK60 alloy (Fig. 14 (e)). It can be inferred that the microstructure immediately after extrusion in ZKX600 alloy would be almost identical to that of ZK60 alloy, although the microstructural evolution was not observed because the butt sample of the extruded ZKX600 alloy did not exist. However, as billet passed through the die, no DRXed grain would have grown despite the presence of frictional heat, unlike the ZK60 alloy.

When the thermal stability of precipitates was identified at 330 °C in the ZKX600 alloy (Fig. 16 (d-f)), a large amount of precipitates remained in the matrix. However, the amount of precipitates was slightly reduced in the heat-treated state of ZKX600 alloy, compared to the as-extruded state. Moreover, fine DRXed grains grew slightly, as shown in Fig. 16 (f). Though TEM analysis of precipitates in Fig. 13, ZKX600 alloy contains not only $MgZn_2$ phase present in ZK60 alloy but also $Ca_2Mg_6Zn_3$ phase. The TEM-EDS results of the ZKX600 alloy (Fig. 13) shows that the fine precipitates contained a small amount of Ca and most of the other precipitates also contained Ca. This indicates that there are smaller amounts of precipitates at 330 °C than those in the as-extruded state because Ca-free $MgZn_2$ precipitate

is almost dissolved into the matrix. Thus, Ca stabilizes these fine precipitates at the elevated temperature of 330 °C. This is in contradiction to the result of thermodynamic calculation in Fig. 15. In fact, thermal stability of the $Ca_2Mg_6Zn_3$ is better than that of the $MgZn_2$ precipitates, suggesting that grain growth can be prevented more effectively when it occurs after recrystallization during extrusion in the ZKX600 alloy, compared to the ZK60 alloy. In addition, it has been reported that fine $Ca_2Mg_6Zn_3$ precipitate is mainly located at DRXed grain boundaries via dynamic precipitation [17, 19, 20]. Therefore, the thermally stable $Ca_2Mg_6Zn_3$ phase was found to exist at grain boundaries, resulting in higher amounts of dynamic precipitates, thus enhancing microstructural homogeneity through Ca addition.

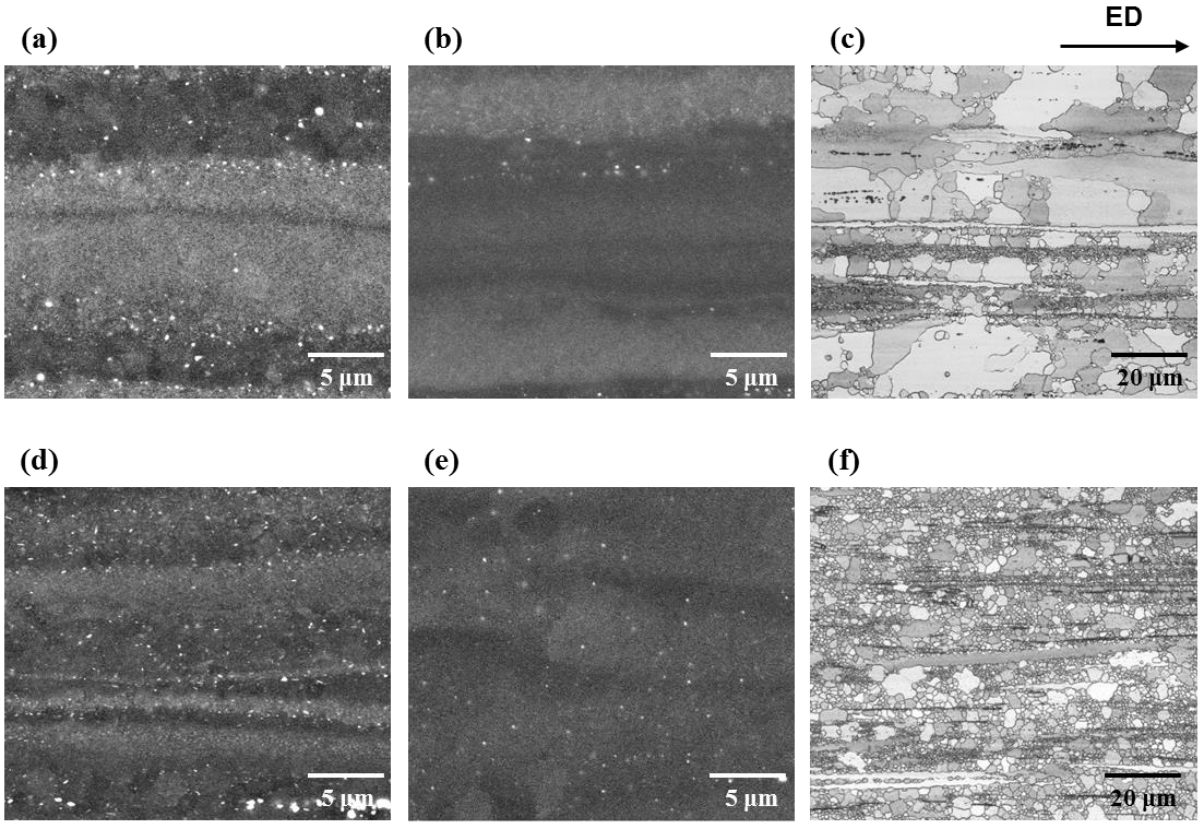

Fig. 16. SEM and optical micrographs of the extruded alloys (a,d) before and (b,c,e,f) after heat-treatment at 330 °C for 2 min: (a-c) ZK60 and (d-f) ZKX600.

Ⅵ. Conclusion

A study has been made on the effect of alloyed Ca on the microstructure of extruded ZK60 Mg alloy with particular emphasis on recrystallization and grain growth during hot extrusion. It was found that alloying with Ca results in the refinement of recrystallized α-Mg grains and also it contributes to enhancing the homogeneity of grain size in the extruded condition. Besides, two different types of second-phase precipitates, $MgZn_2$ and $Ca_2Mg_6Zn_3$, were found to exist in the Ca-containing ZKX600 alloy, although only $MgZn_2$ precipitates appeared in the ZK60 alloy without alloyed Ca. Microstructural examinations for the extruded alloys after artificial heat-treatment at 330 °C indicated that such microstructural changes in grain size and its homogeneity by Ca addition can result from the thermal stability of the $Ca_2Mg_6Zn_3$ precipitates, which is better than that of the $MgZn_2$ precipitates, suggestive of more effective inhibition of grain growth occurring after recrystallization during hot extrusion in the ZKX600 alloy relative to the ZK60 alloy without the $Ca_2Mg_6Zn_3$ precipitates.

Ⅶ. References

[1] C. J. Bettles and M. A. Gibson, "Current wrought magnesium alloys; strength and weakness," *JOM,* vol. 57, no. 5, pp. 46-49, 2005.

[2] N. J. Kim, "Critical Assessment 6: Magnesium sheet alloys: viable alternatives to steels?," *Materials Science and Technology,* vol. 30, no. 15, pp. 1925-1928, 2014.

[3] A. A. Luo and A. K. Sachdev, "Applications of magnesium alloys in automotive engineering," pp. 393-426, 2012.

[4] B. L. Mordike and T. Ebert, "Magnesium Properties-applications-potential," *Materials Science and Engineering: A,* vol. A302, pp. 37-45, 2001.

[5] K. Hono, C. L. Mendis, T. T. Sasaki, and K. Oh-ishi, "Towards the development of heat-treatable high-strength wrought Mg alloys," (in English), *Scripta Materialia,* vol. 63, no. 7, pp. 710-715, Oct 2010.

[6] J.-F. Nie, "Physical Metallurgy of Light Alloys," pp. 2009-2156, 2014.

[7] H. Y. Jeong, B. Kim, S. G. Kim, H. J. Kim, and S. S. Park, "Effect of Ce addition on the microstructure and tensile properties of extruded Mg–Zn–Zr alloys," *Materials Science and Engineering: A,* vol. 612, pp. 217-222, 2014.

[8] E. F. Emley, *Principles of magnesium technology*. Oxford; New York: Pergamon Press, 1966.

[9] T. Bhattacharjee, T. Nakata, T. T. Sasaki, S. Kamado, and K. Hono, "Effect of microalloyed Zr on the extruded microstructure of Mg–6.2Zn-based alloys," *Scripta Materialia,* vol. 90-91, pp. 37-40, 2014.

[10] Y. Z. Du, X. G. Qiao, M. Y. Zheng, D. B. Wang, K. Wu, and I. S. Golovin, "Effect of microalloying with Ca on the microstructure and mechanical properties of Mg-6 mass%Zn alloys," *Materials & Design,* vol. 98, pp. 285-293, 2016.

[11] B. Zhang, Y. Wang, L. Geng, and C. Lu, "Effects of calcium on texture and mechanical properties of hot-extruded Mg–Zn–Ca alloys," *Materials Science and Engineering: A,* vol. 539, pp. 56-60, 2012.

[12] L. B. Tong, M. Y. Zheng, L. R. Cheng, S. Kamado, and H. J. Zhang, "Effect of extrusion ratio on microstructure, texture and mechanical properties of indirectly extruded Mg–Zn–Ca alloy," *Materials Science and Engineering: A,* vol. 569, pp. 48-53, 2013.

[13] Q. Wen, K.-k. Deng, J.-y. Shi, B.-p. Zhang, and W. Liang, "Effect of Ca addition on the microstructure and tensile properties of Mg–4.0Zn–2.0Gd alloys," *Materials Science and Engineering: A,* vol. 609, pp. 1-6, 2014.

[14] S. Kamrani and C. Fleck, "Effects of calcium and rare-earth elements on the microstructure and tension–compression yield asymmetry of ZEK100 alloy," *Materials Science and Engineering: A,* vol. 618, pp. 238-243, 2014.

[15] H. Ding, X. Shi, Y. Wang, G. Cheng, and S. Kamado, "Texture weakening and ductility variation of Mg–2Zn alloy with CA or RE addition," *Materials Science and Engineering: A,* vol. 645, pp. 196-204, 2015.

[16] L. B. Tong *et al.*, "Influence of deformation rate on microstructure, texture and mechanical properties of indirect-extruded Mg–Zn–Ca alloy," *Materials Characterization,* vol. 104, pp. 66-72, 2015.

[17] W.-j. Li, K.-k. Deng, X. Zhang, K.-b. Nie, and F.-j. Xu, "Effect of ultra-slow extrusion speed on the microstructure and mechanical properties of Mg-4Zn-0.5Ca alloy," *Materials Science and Engineering: A,* vol. 677, pp. 367-375, 2016.

[18] P. M. Jardim, G. Solórzano, and J. B. V. Sande, "Second phase formation in melt-spun Mg–Ca–Zn alloys," *Materials Science and Engineering: A,* vol. 381, no. 1-2, pp. 196-205, 2004.

[19] T. V. Larionova, W.-W. Park, and B.-S. You, "A ternary phase observed in rapidly solidified Mg-Ca-Zn alloys," *Scripta Materialia,* vol. 45, pp. 7-12, 2001.

[20] S. W. Xu, K. Oh-ishi, H. Sunohara, and S. Kamado, "Extruded Mg–Zn–Ca–Mn alloys with low yield anisotropy," *Materials Science and Engineering: A,* vol. 558, pp. 356-365, 2012.

[21] A. C. Hänzi *et al.*, "Design strategy for microalloyed ultra-ductile magnesium alloys," *Philosophical Magazine Letters,* vol. 89, no. 6, pp. 377-390, 2009.

[22] P. A. Manohar, M. Ferry, and T. Chandra, "Five Decades of the Zener Equation," *ISIJ International,* vol. 38, no. 9, pp. 913-924, 1998.

[23] C. Bettles, "Enhanced age-hardening behaviour in Mg-4 wt.% Zn micro-alloyed with Ca," *Scripta Materialia,* vol. 51, no. 3, pp. 193-197, 2004.

[24] C. Ma, M. Liu, G. Wu, W. Ding, and Y. Zhu, "Tensile properties of extruded ZK60–RE alloys," *Materials Science and Engineering: A,* vol. 349, no. 1-2, pp. 207-212, 2003.

[25] S. M. He, L. M. Peng, X. Q. Zeng, W. J. Ding, and Y. P. Zhu, "Comparison of the microstructure and mechanical properties of a ZK60 alloy with and without 1.3wt.% gadolinium addition," *Materials Science and Engineering: A,* vol. 433, no. 1-2, pp. 175-181, 2006.

[26] H. T. Zhou, Z. D. Zhang, C. M. Liu, and Q. W. Wang, "Effect of Nd and Y on the microstructure and mechanical properties of ZK60 alloy," *Materials Science and Engineering: A,* vol. 445-446, pp. 1-6, 2007.

[27] W. Yu, Z. Liu, H. He, N. Cheng, and X. Li, "Microstructure and mechanical properties of ZK60–Yb magnesium alloys," *Materials Science and Engineering: A,* vol. 478, no. 1-2, pp. 101-107, 2008.

[28] F.-s. Pan, T.-t. Liu, X.-y. Zhang, A.-t. Tang, and W.-q. Wang, "Effects of scandium addition on microstructure and mechanical properties of ZK60 alloy," *Progress in Natural Science: Materials International,* vol. 21, no. 1, pp. 59-65, 2011.

[29] T. Liu, F. Pan, and X. Zhang, "Effect of Sc addition on the work-hardening behavior of ZK60 magnesium alloy," *Materials & Design,* vol. 43, pp. 572-577, 2013.

[30] H. Yu, S. Hyuk Park, B. Sun You, Y. Min Kim, H. Shun Yu, and S. Soo Park, "Effects of extrusion speed on the microstructure and mechanical properties of ZK60 alloys with and without 1wt% cerium addition," *Materials Science and Engineering: A,* vol. 583, pp. 25-35, 2013.

[31] H. Yu, Y. M. Kim, B. S. You, H. S. Yu, and S. H. Park, "Effects of cerium addition on the microstructure, mechanical properties and hot workability of ZK60 alloy," *Materials Science and Engineering: A,* vol. 559, pp. 798-807, 2013.

[32] B. Chen and J. Zhang, "Microstructure and mechanical properties of ZK60-Er magnesium alloys," *Materials Science and Engineering: A,* vol. 633, pp. 154-160, 2015.

[33] L. Liu *et al.*, "Microstructure, texture, mechanical properties and electromagnetic shielding effectiveness of Mg–Zn–Zr–Ce alloys," *Materials Science and Engineering: A,* vol. 669, pp. 259-268, 2016.

[34] L. B. Tong *et al.*, "Microstructure and mechanical properties of Mg–Zn–Ca alloy processed by equal channel angular pressing," *Materials Science and Engineering: A,* vol. 523, no. 1-2, pp. 289-294, 2009.

[35] R. Zheng *et al.*, "Simultaneously enhanced strength and ductility of Mg-Zn-Zr-Ca alloy with fully recrystallized ultrafine grained structures," *Scripta Materialia,* vol. 131, pp. 1-5, 2017.

[36] H. E. Friedrich and B. L. Mordike, "Magnesium Technology," *Springer,* pp. 300-301, 2006.

[37] F. J. Humphreys and M. Hatherly, "Recrystallization and Related Annealing Phenomena," pp. 415-450, 2004.

[38] K. Oh-ishi, C. L. Mendis, T. Homma, S. Kamado, T. Ohkubo, and K. Hono, "Bimodally grained microstructure development during hot extrusion of Mg–2.4 Zn–0.1 Ag–0.1 Ca–0.16 Zr (at.%) alloys," *Acta Materialia,* vol. 57, no. 18, pp. 5593-5604, 2009.

[39] A. G. Beer, "Enhancing the extrudability of wrought magnesium alloys," pp. 304-322, 2012.

[40] T. Bhattacharjee, C. L. Mendis, T. T. Sasaki, T. Ohkubo, and K. Hono, "Effect of Zr addition on the precipitation in Mg–Zn-based alloy," *Scripta Materialia,* vol. 67, no. 12, pp. 967-970, 2012.

[41] C. L. Mendis, K. Oh-ishi, and K. Hono, "Enhanced age hardening in a Mg–2.4at.% Zn alloy by trace additions of Ag and Ca," *Scripta Materialia,* vol. 57, no. 6, pp. 485-488, 2007.

[42] B. Kim, S.-M. Baek, H. Y. Jeong, J. G. Lee, and S. S. Park, "Grain refinement and reduced yield asymmetry of extruded Mg–5Sn–1Zn alloy by Al addition," *Journal of Alloys and Compounds,* vol. 660, pp. 304-309, 2016.

[43] D. A. Porter, K. E. Easterling, and M. Sherif, *Phase Transformations in Metals and Alloys, Third Edition*. CRC Press, 2009.

[44] S. Farahany, H. R. Bakhsheshi-Rad, M. H. Idris, M. R. Abdul Kadir, A. F. Lotfabadi, and A. Ourdjini, "In-situ thermal analysis and macroscopical characterization of Mg–xCa and Mg–0.5Ca–xZn alloy systems," *Thermochimica Acta,* vol. 527, pp. 180-189, 2012.

[45] Y.-N. Zhang, D. Kevorkov, J. Li, E. Essadiqi, and M. Medraj, "Determination of the solubility range and crystal structure of the Mg-rich ternary compound in the Ca–Mg–Zn system," *Intermetallics,* vol. 18, no. 12, pp. 2404-2411, 2010.

[46] Y. N. Zhang, D. Kevorkov, F. Bridier, and M. Medraj, "Experimental study of the Ca-Mg-Zn system using diffusion couples and key alloys," *Sci Technol Adv Mater,* vol. 12, no. 2, p. 025003, Apr 2011.

[47] J. Bohlen, S. B. Yi, J. Swiostek, D. Letzig, H. G. Brokmeier, and K. U. Kainer, "Microstructure and texture development during hydrostatic extrusion of magnesium alloy AZ31," *Scripta Materialia,* vol. 53, no. 2, pp. 259-264, 2005.

[48] B. Kim, S.-M. Baek, J. G. Lee, and S. S. Park, "Enhanced strength and plasticity of Mg–6Zn–0.5Zr alloy by low-temperature indirect extrusion," *Journal of Alloys and Compounds,* vol. 706, pp. 56-62, 2017.